NASA/TM—2012-217631 SPIE83452G

Optimal Topology and Experimental Evaluation of Piezoelectric Materials for Actively Shunted General Electric Polymer Matrix Fiber Composite Blades

Benjamin B. Choi
Glenn Research Center, Cleveland, Ohio

Kirsten Duffy
The University of Toledo, Toledo, Ohio

Jeffrey L. Kauffman
The Pennsylvania State University, University Park, Pennsylvania

Nicholas Kray
GE Aviation, Cincinnati, Ohio

December 2012

NASA STI Program . . . in Profile

Since its founding, NASA has been dedicated to the advancement of aeronautics and space science. The NASA Scientific and Technical Information (STI) program plays a key part in helping NASA maintain this important role.

The NASA STI Program operates under the auspices of the Agency Chief Information Officer. It collects, organizes, provides for archiving, and disseminates NASA's STI. The NASA STI program provides access to the NASA Aeronautics and Space Database and its public interface, the NASA Technical Reports Server, thus providing one of the largest collections of aeronautical and space science STI in the world. Results are published in both non-NASA channels and by NASA in the NASA STI Report Series, which includes the following report types:

- TECHNICAL PUBLICATION. Reports of completed research or a major significant phase of research that present the results of NASA programs and include extensive data or theoretical analysis. Includes compilations of significant scientific and technical data and information deemed to be of continuing reference value. NASA counterpart of peer-reviewed formal professional papers but has less stringent limitations on manuscript length and extent of graphic presentations.

- TECHNICAL MEMORANDUM. Scientific and technical findings that are preliminary or of specialized interest, e.g., quick release reports, working papers, and bibliographies that contain minimal annotation. Does not contain extensive analysis.

- CONTRACTOR REPORT. Scientific and technical findings by NASA-sponsored contractors and grantees.

- CONFERENCE PUBLICATION. Collected papers from scientific and technical conferences, symposia, seminars, or other meetings sponsored or cosponsored by NASA.

- SPECIAL PUBLICATION. Scientific, technical, or historical information from NASA programs, projects, and missions, often concerned with subjects having substantial public interest.

- TECHNICAL TRANSLATION. English-language translations of foreign scientific and technical material pertinent to NASA's mission.

Specialized services also include creating custom thesauri, building customized databases, organizing and publishing research results.

For more information about the NASA STI program, see the following:

- Access the NASA STI program home page at *http://www.sti.nasa.gov*

- E-mail your question to *help@sti.nasa.gov*

- Fax your question to the NASA STI Information Desk at 443–757–5803

- Phone the NASA STI Information Desk at 443–757–5802

- Write to:
  STI Information Desk
  NASA Center for AeroSpace Information
  7115 Standard Drive
  Hanover, MD 21076–1320

NASA/TM—2012-217631 SPIE83452G

Optimal Topology and Experimental Evaluation of Piezoelectric Materials for Actively Shunted General Electric Polymer Matrix Fiber Composite Blades

Benjamin B. Choi
Glenn Research Center, Cleveland, Ohio

Kirsten Duffy
The University of Toledo, Toledo, Ohio

Jeffrey L. Kauffman
The Pennsylvania State University, University Park, Pennsylvania

Nicholas Kray
GE Aviation, Cincinnati, Ohio

Prepared for the
Smart Structures and Materials and Nondestructive Evaluation and Health Monitoring 2012
sponsored by the International Society for Optical Engineering (SPIE)
San Diego, California, March 11–15, 2012

National Aeronautics and
Space Administration

Glenn Research Center
Cleveland, Ohio 44135

December 2012

Acknowledgments

This work was in support of a Space Act Agreement with GE Aviation and part of NASA's Subsonic Fixed Wing (SFW) project. It was funded by the Fundamental Aeronautics Program. Test articles were provided by GE Aviation, and testing was performed at NASA Glenn. The authors extend their thanks to Mr. Andrew Provenza at NASA Glenn for his great efforts in operating the Dynamic Spin Rig during testing.

This work was sponsored by the Fundamental Aeronautics Program
at the NASA Glenn Research Center.

Level of Review: This material has been technically reviewed by technical management.

Available from

NASA Center for Aerospace Information
7115 Standard Drive
Hanover, MD 21076–1320

National Technical Information Service
5301 Shawnee Road
Alexandria, VA 22312

Available electronically at http://www.sti.nasa.gov

Optimal Topology and Experimental Evaluation of Piezoelectric Materials for Actively Shunted General Electric Polymer Matrix Fiber Composite Blades

Benjamin B. Choi
National Aeronautics and Space Administration
Glenn Research Center
Cleveland, Ohio 44135

Kirsten Duffy
The University of Toledo
Toledo, Ohio 43606

Jeffrey L. Kauffman
The Pennsylvania State University
University Park, Pennsylvania 16802

Nicholas Kray
GE Aviation
Cincinnati, Ohio 45215

Summary

NASA Glenn Research Center, in collaboration with GE Aviation, has begun the development of a smart adaptive structure system with piezoelectric (PE) transducers to improve composite fan blade damping at resonances. Traditional resonant damping approaches may not be realistic for rotating frame applications such as engine blades. The limited space in which the blades reside in the engine makes it impossible to accommodate the circuit size required to implement passive resonant damping. Thus, a novel digital shunt scheme has been developed to replace the conventional electric passive shunt circuits. The digital shunt dissipates strain energy through the load resistor on a power amplifier. General Electric (GE) designed and fabricated a variety of polymer matrix fiber composite (PMFC) test specimens. Investigating the optimal topology of PE sensors and actuators for each test specimen has revealed the best PE transducer location for each target mode. Also a variety of flexible patches, which can conform to the blade surface, have been tested to identify the best performing PE patch. The active damping control achieved significant performance at target modes. This work has been highlighted by successful spin testing up to 5000 rpm of subscale GEnx composite blades in Glenn's Dynamic Spin Rig.

Introduction

Previously, NASA Glenn Research Center developed several damping technologies to reduce excessive vibratory stresses that led to high-cycle fatigue (HCF) failures in aircraft engine turbomachinery. These activities included viscoelastic damping by Mehmed and Kosmatka (Ref. 1), passive impact damping by Duffy (Ref. 2), plasma sprayed damping coating, and high-temperature shape memory alloy (Ref. 3).

Recently, in support of a Space Act Agreement with GE Aviation and as part of NASA's Subsonic Fixed Wing (SFW) Project, Glenn's researchers have been investigating a new damping technology for composite fan blades for future aircraft designed to achieve a higher level of aerodynamic performance. As a means of reducing engine blade vibration, piezoelectric (PE) blade damping has been proposed to support part of the project's goals such as lighter, quieter, and fuel-efficient composite fans for

turbomachinery applications. GE has designed and instrumented a variety of polymer matrix fiber composite (PMFC) test specimens, including subscale GEnx fan blades. For PMFC blades, the piezoelectric (PE) elements could be embedded within the blade material, protecting the brittle PE material from the airflow and minimizing aerodynamic performance degradation.

In the past few decades, it has become evident that PE shunt damping is a promising technology for suppressing significant mechanical vibration at structural modes. The principle of PE shunt damping is that PE materials can convert mechanical energy into electrical energy, and the electrical energy can be dissipated through a connected load resistor of a power amplifier. Hagood and von Flotow (Ref. 4) first presented an analytical model for resistive and inductive-resistive shunt dampened systems, showing that the resonant shunt behaves like a mechanical vibration absorber. Since then, many researchers have begun to further develop PE damping with tests and analyses. Lesieutre (Ref. 5) described the different types of shunt circuits and how they affect vibration behavior.

In recent advances in the turbomachinery applications, Cross and Fleeter (Ref. 6) developed a passive control for turbomachine blading flow-induced vibrations, and employed a synthetic inductor that replaced a large size inductor to control the first bending mode of the PE blade. Livet (Ref. 7) tested a virtual inductor for compressor disk blade damping control. Numerous papers for passive shunt development in turbomachinery applications have been published, and most of them have dealt with analog semipassive circuits that consist of operational amplifiers (op-amps), resistors, gyrators, and an external power supply.

Some researchers have used an active control approach for the PE actuators for turbomachinery blade vibration control. Remington (Ref. 8) reduced low-speed fan noise control using actively controlled PE actuators mounted on stator vanes. Watanabe (Ref. 9) used a traditional feedback control scheme to oscillate the PE patches for cascade flutter control in subsonic flow. In 2009, NASA Ames and Boeing (Ref. 10) developed and successfully demonstrated a civilian, full-scale MD 900 Explorer helicopter rotor (SMART rotor) with on-blade PE actuators that have a conventional controller driving the trailing edge flaps. This wind-tunnel testing obviated a controversial issue concerning the use of PE materials to generate enough force to excite the rotating blades. This experiment motivated us to continue the PE damping of high-speed turbomachinery fan blades.

However, the aforementioned semipassive damping approaches may not be viable for rotating frame applications such as engine blades. The limited space in which the blades reside in the engine makes it impossible to accommodate the circuit size required to implement damping. Additionally, there is the risk of rotor imbalance with operation at high-centrifugal loads. Further, the active control approach using proportional-integral-derivative (PID) controller law, used by most researchers, is not effective for resonant vibration suppression.

In this report, therefore, a novel digital shunt scheme to replace the conventional electric passive shunt circuits is presented. The digital shunt dissipates strain energy through the load resistor on a power amplifier. The feasibility and effectiveness of using PE materials to suppress the resonant vibrations of composite test specimens is then investigated by testing several off-the-shelf PE patches with different material properties to identify the best performing PE actuators and sensors for actively controlled test specimens. In this work, GE designed and fabricated a variety of PMFC test specimens: wide and narrow beams for surface-mounted PE transducers as well as small subscale GEnx composite fan blades for spin testing.

After selecting the best PE patches, the Glenn team continued to investigate the optimal topology of PE sensors and actuators for the subscale GEnx composite fan blades. Finally, Glenn's Dynamic Spin Rig (DSR) test results of subscale GEnx blades with PE patches at 0 to 5000 rpm in vacuum is presented here.

Symbols

A controller transfer function
C capacitance
d distance from blade base to position where external force is applied

F external force
G transfer function
L inductance
Q quality factor
R resistance
r distance where displacement is measured
TF transfer function
V voltage
Y displacement
Z impedance
η loss factor
ζ critical damping ratio
ω circular frequency

Subscripts:

a	actuator
ac	active control
b	baseline
fv	actuator voltage with respect to external force
fy	displacement with respect to external force
in	input
out	output
PEB_base	patch PE B to base excitation
p	PE patch
s	sensor
tip_base	blade tip to base excitation
vv	sensor voltage with respect to actuator voltage
vy	displacement with respect to sensor voltage

Shunt Damping and Digital Control Design

PE materials, because of their lightness and easy integration into the host structure, have been extensively employed in vibration-control schemes used in aeronautics and aerospace structures. Strategies for vibration control include passive and active concepts.

Passive Resistive-Inductive (*RL*) Shunt

Passive vibration damping is intrinsically stable and cheap and is easily implemented by using PE actuators. In general, the actuators are bonded to the mechanical structure and shunted to suitable external circuits, containing resistive and inductive components that dissipate electric energy. That is, the PE patch, shunted through a *RL* circuit, acts as a vibration absorber, which is tuned to the same frequency of the motion to be damped. The *RL* series circuit is generally accepted as one the best passive shunts for vibration damping of a single mode or multimodes (Refs. 4, 5, 11, and 12).

However, a major problem with using this approach arises from the large inductor size and mass for the low-frequency-tuned resonant circuit that is needed when the mechanical frequency of interest is low. Consequently, many researchers have proposed the use of synthetic inductors (Refs. 6 and 7) to reduce the weight and volume of the circuits. It required a constant power supply, and its size was still considerably large. Nevertheless, the *RL* shunt or synthetic inductor is suitable for stationary frame applications. For turbomachinery applications, however, an implementation issue can arise when applied to the limited space in which the blades reside in the engine. Further, there is the risk of rotor imbalance during operation at high-centrifugal loads.

Digital Control Design

As an alternative to the passive *RL* shunt, Choi (Refs. 13 and 14) developed a new active control approach that replaces equivalent passive-shunt analog circuits with a digital code. His controller demonstrated significant resonance damping performance when used on titanium-alloy flat plates (Ref. 13) and titanium-alloy fan blades (Ref. 14). For dynamic spin testing, the blade's natural frequencies will vary as a function of the shaft's rotation speed. Thus, a real-time adaptive feature to follow changes in the blade's natural frequencies must be developed to generate adaptive controller tuning in real time to the changing condition.

Figure 1(a) shows a general feedback control of analog *RLC* (resistive-inductive-capacitive) network. Its transfer function (Ref. 15) can be described as

$$Z_{\text{in}} = R + i\omega L - i/(\omega C) \tag{1}$$

$$Z_{\text{out}} = R + i\omega L \tag{2}$$

$$\frac{V_{\text{out}}}{V_{\text{in}}} = \frac{Z_{\text{out}}}{Z_{\text{in}}} = \frac{R + i\omega L}{R + i\omega L - i/(\omega C)} = \frac{Cs(R + Ls)}{LCs^2 + CRs + 1} \tag{3}$$

where Z_{in} and Z_{out} are the impedance input and output, respectively; ω is the circular frequency; V_{out} and V_{in} are the voltage output and input, respectively; and s represents the complex frequency domain.

As shown in Equation (3), the transfer function of the feedback controller is expressed in terms of passive circuit components (*RLC*) regardless of modal shape. Figure 1(b) shows a block diagram of active feedback controller. The sensor voltage signal $V_s(s)$ is fed back to the transfer function and the actuator control signal; hence,

$$V_a(s) = -A_i(s)V_s(s) + V_{\text{in}}(s) \tag{4}$$

where A_i is the ith controller transfer function,

$$A_i(s) = Cs(R_i + L_i s)/(L_i Cs^2 + CR_i s + 1) \tag{5}$$

Also, V_s is the sensor voltage and V_{in} is the voltage input. This control law is completely different from PID control law, which has been used for the active PE damping control done by many researchers (Refs. 7 to 10). It is of interest to note that multimode control, using only one actuator patch, might be possible if the single patch can excite the target multimodes sufficiently. A set of control laws for each target mode shown in Equation (5) are mathematically summed and can be applied as a single control command to the single actuator patch.

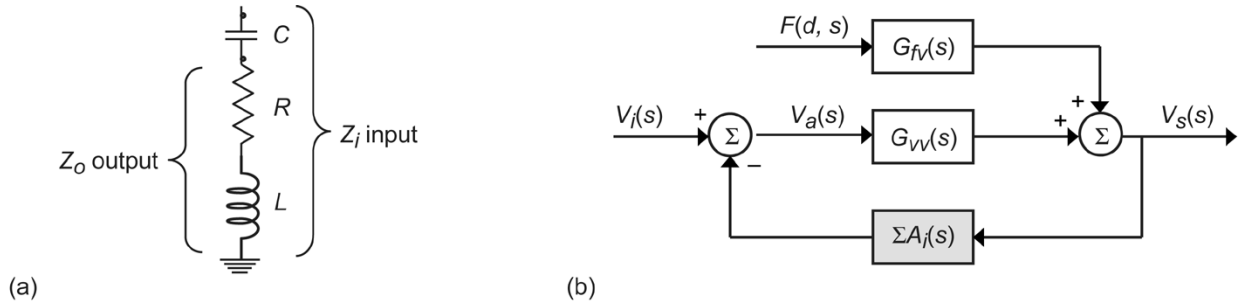

Figure 1.—Feedback control architecture. Z_O is impedance output; Z_i, impedance input; C, capacitance; R, resistance; L, inductance; $F(d,s)$, external force; $G_{fV}(s)$, transfer function with respect to sensor voltage; Σ, summation of all individual control currents; $V_a(s)$, actuator voltage; $G_{VV}(s)$, transfer function of actuator voltage with respect to sensor voltage; $V_s(s)$, sensor voltage; and $A_i(s)$, controller transfer function. (a) General feedback control *RLC* network. (b) Feedback block diagram for blade structure with piezoelectrics.

In Figure 1(b), the closed-loop system performance of sensor voltage and displacement, respectively, are

$$V_s(s) = \frac{G_{fv}(s)F(d,s)}{1 + A(s)G_{vv}(s)} + \frac{G_{vv}(s)V_i(s)}{1 + A(s)G_{vv}(s)} \tag{6}$$

$$Y(r,s) = \frac{G_{fy}(r,s)F(d,s)}{1 + A(s)G_{vv}(s)} + \frac{G_{vy}(r,s)V_i(s)}{1 + A(s)G_{vv}(s)} \tag{7}$$

where

$$G_{fv}(s) = \frac{V_a(s)}{F(d,s)}, G_{vv}(s) = \frac{V_s(s)}{V_a(s)} \tag{8}$$

$$G_{fy}(r,s) = \frac{Y(r,s)}{F(d,s)}, G_{vy}(s) = \frac{Y(r,s)}{V_a(s)} \tag{9}$$

Note

G_{fv} transfer function of the actuator voltage with respect to external force
G_{fy} transfer function of displacement with respect to external force, G_{vv} is the transfer function of sensor voltage with respect to actuator voltage
G_{fy} transfer function of displacement with respect to external force
G_{vy} transfer function of displacement with respect to sensor voltage
F external force
d distance from the blade base to the position where the external force is applied
Y displacement
r distance from the blade base to where displacement is measured

The transfer functions in Equations (8) and (9) can be obtained by using MATLAB (The MathWorks, Inc.) software based on the experimental system frequency response. A spectrum analyzer was used to obtain experimental measurement of the test specimen's modal frequency response. The MATLAB Frequency Domain System software identifies the linear dynamic transfer function of a single-input/single-output (SISO) system. Finally, by using the Symbolic Math Toolbox, a complete mathematical model of the closed-loop system in Equations (6) and (7) can be derived, where the control law is described in Equation (5).

The inductor value L_i is chosen for the particular (target) frequency ω_i as

$$\omega_i = \frac{1}{\sqrt{L_i C_{pi}}} \tag{10}$$

where the value of C_{pi} is the capacitance of the PE patch in farads. The resistor value R is chosen to optimize the damping over a frequency bandwidth. In general, increasing the R value means good damping, but high control power consumption. Thus, the optimized R value must be selected by taking into account the test equipment specifications.

Simulation Results

To assess the merit of the active damping control, a number of simulations of open- and closed-loop transfer functions were performed on a simply supported beam with bonded PE transducers. For this simulation study, a six-mode truncated mathematical model was constructed (Fig. 2), assuming the values

of the resonant frequencies and damping ratios of the PE beam. It was also assumed that six pairs of collocated PE actuator and sensor patches were needed; these were placed on the optimal locations to control the six target modes. The digital shunt control technique (described in the upcoming section, "Optimal Patch Selection") was then employed to determine the feedback control laws for the optimal parallel and series shunt circuits for the target resonances. Damping performance was evaluated by measuring the open- and closed-loop frequency responses (Fig. 3(a)) and time history (Fig. 3(b)) of the PE beam.

The simulation results showed that the active controller significantly reduced the vibrations of the beam, pushing the resonant peaks down. Notice that unlike PID control law, this feedback is effective at targeted blade frequencies only. It was concluded that a transfer function of the *RLC* shunt circuit can be expressed in S-domain as in Equation (4), so that it can be programmed in a digital code. Further, a real-time adaptive control for change in blade frequencies for spin testing can be implemented, as opposed to the analog shunt circuit approach.

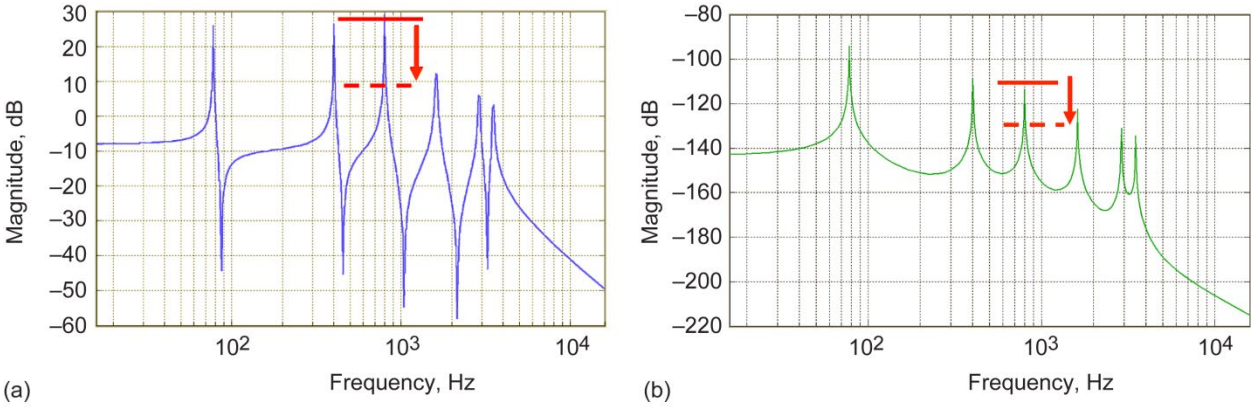

Figure 2.—Open-loop frequency responses. (a) Bode plot of transfer function of actuator voltage with respect to sensor voltage, G_{VV}. (b) Bode plot of transfer function of sensor voltage with respect to displacement, G_{VY}.

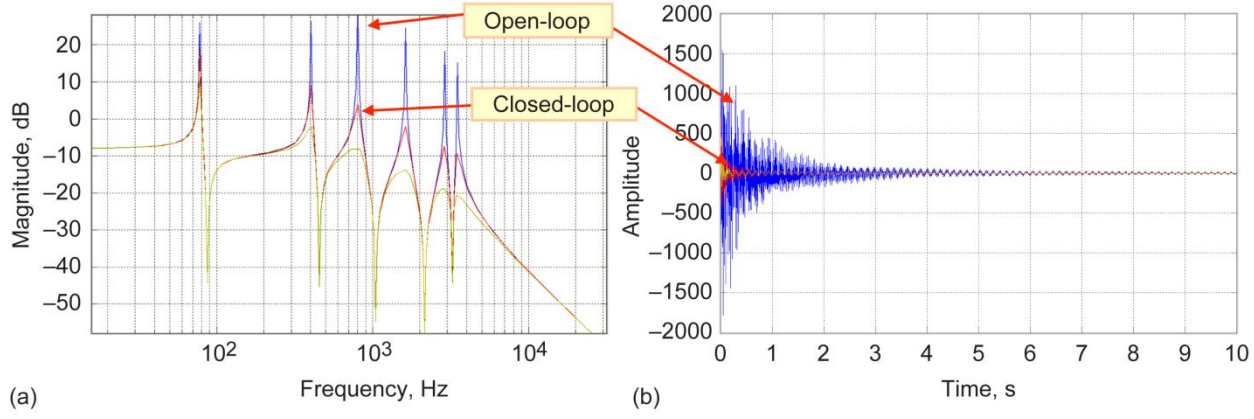

Figure 3.—Open- and closed-loop responses of the transfer function of actuator voltage with respect to sensor voltage, G_{VV}.

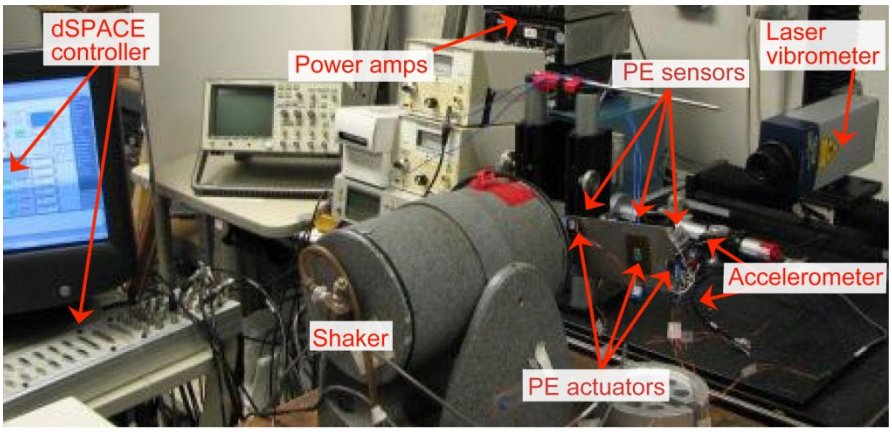

Figure 4.—Experimental setup for piezoelectric (PE) patch bench test.

Bench Test Setup

Figure 4 shows the experimental bench test setup. For baseline (open-loop) testing, the test specimen was excited with a frequency sweep through target resonance using a spectrum analyzer. The base excitation level and the tip response were measured using accelerometers. The resonance frequency and damping are then calculated from the experimental transfer function of the tip response to the base excitation.

For the active control (closed-loop) testing, Simulink and the Real Time Workshop for MATLAB are used to generate C code for the digital shunt control laws, and the executable control code is downloaded into the dSPACE control system to implement the digital shunt. The accelerometer signal of the tip displacement is fed back to the dSPACE control system that generates the control command signal. The power amplifier magnifies the signal and delivers power to energize the PE patches on the test specimen. The closed-loop transfer function of the tip response to that of the base acceleration is measured to calculate the active damping performance. Here, the value for L is chosen to target a particular frequency, and the value for R is chosen to optimize the damping over the target frequency band. The closed-loop gain is carefully selected to meet the damping requirement within the feedback stability margin. In practice, the entire control system can be implemented on a powered chip on the rotating frame if DC power can be supplied to energize the power electronics.

Experimental Evaluation of PE Materials

The goal of this section is to investigate the ability and effectiveness of using PE materials to damp resonant vibrations of GE-made graphite/epoxy composite coupons. It is then determined which type of PE patch generates the best performance in terms of damping and required control power consumption. A variety of commercially available PE materials were tested to identify the optimally performing sensor and actuator for nonrotating vibration reduction.

Tested PE Materials

All tests were performed on PMFC test specimens with surface-mounted PE elements. Table I describes the material properties of the different patch types that were used in the test. Evaluated PE patches are Midé nonflexible, Smart Material (S–M) flexible d_{31} and d_{33} types, and Advanced Cerametrics flexible d_{33}-type patches. The PE patches all incorporate Navy Type-II lead zirconium titanate (PZT-5A, Annon Piezo Technology Co., Ltd.) material.

TABLE I.—MATERIAL PROPERTIES OF PIEZOELECTRIC PATCHES

Patch	Type	Dimensions, in^3	Capacitance, C, μF	Maximum voltage, V_{max}, V	Maximum force, F_{max}, lbf
Midé QP10w	Flat, d_{31}	1.81 by 1.310 by 0.010	105	±200	15
Smart Material (S–M) M2814–P1	Flexible, d_{33}	1.10 by 0.600 by 0.012	0.61	–500 to 1500	195
S–M M2814–P2	Flexible, d_{31}	1.10 by 0.600 by 0.012	25.7	–60 to 360	85
S–M M0714–P2	Flexible, d_{31}	0.275 by 0.30 by 0.012	6.5	–60 to 360	85
Advanced Cerametrics	Flexible, d_{33}	0.275 by 0.27 by N/A	0.95	–60 to 360	N/A

Optimal Patch Selection

PE patches were tested on the two composite coupons: narrow and wide cantilever composite beams. The dimension of the narrow beam is 9.5 by 1.30 by 0.25 in.; the wide beam is 9.5 by 2.0 by 0.25 in. Each beam length of 2.0 in. at one end was inserted into the shaker armature clamp so that 7.5 in. extended from the clamp. PE patches were surface mounted with Duralco 4537N epoxy (Cotronics Corp.) near the base of the test specimens. This location was optimal for the actuator patch at the first bending site, which was of interest in this work.

We began bench testing the Advanced Cerametrics d_{33} type versus S–M's M2814-P1d_{33} type on the narrow beam. As shown in Figure 5, each patch was placed 2.0 in. (clamp area) from one end of the narrow beam, and one accelerometer was mounted at the blade tip for the displacement measurement. The target resonance of this test was the first bending mode, around 162.5 Hz. The HP analyzer generated a swept sine signal that was used to excite the beam through the target mode as well as experimental open- and closed-loop transfer functions of the tip response relative to the base excitation. Damping was calculated from this data.

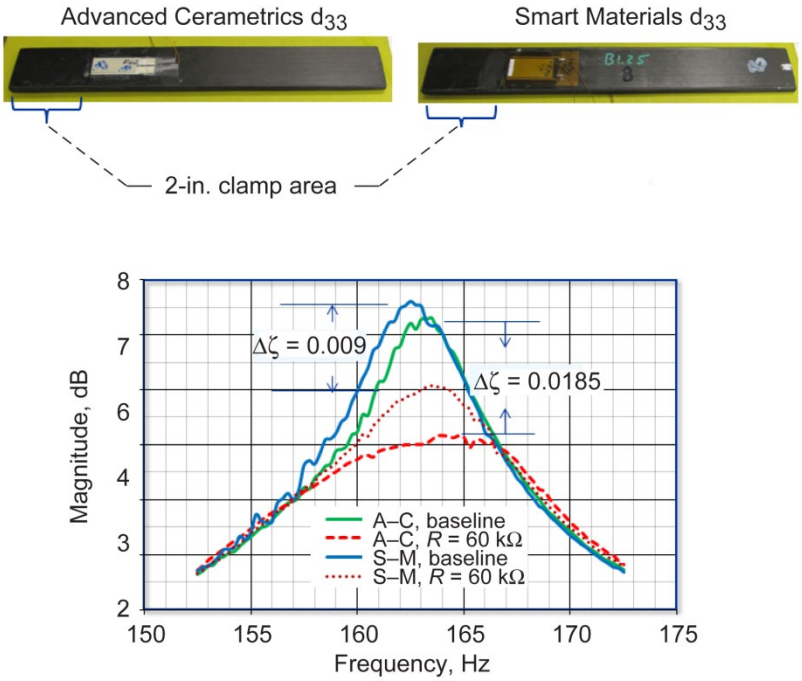

Figure 5.—Bode plot of transfer functions around first bending mode (narrow beam), using Advanced Cerametrics (A–C) and Smart Material (S–M) d_{33} piezoelectric patches. Δζ represents the increase in damping.

We first measured baseline damping without the control system ζ_b and then damping with active vibration control ζ_{ac} so that the added damping can be calculated as $\Delta\zeta = \zeta_{ac} - \zeta_b$. Figure 5 shows the Bode plot of the open- and closed-loop transfer functions of using the two different patches. With the same controller setup, the Advanced Cerametrics d_{33}-type patch produced $\Delta\zeta = 0.0185$, and the S–M d_{33} type produced $\Delta\zeta = 0.009$. In general, the assumed target damping is $\zeta_{ac} > 0.005$ (i.e., loss factor $\eta > 0.01$ and quality factor $Q < 100$). However, the problem with this type of bench testing configuration is that the first bending mode had already high damping of $\zeta_{ac} \cong 0.02$. Nevertheless, both actuator patches achieved, surprisingly, significant damping capabilities at the target mode of 162.5 Hz. This kind of low-frequency damping has been considered to be a significant challenge because of difficult implementation.

Another factor in determining the best performing patch candidate is the required control power consumption for the added damping performance. Figure 6 shows that the required control effort in using the Advanced Cerametrics d_{33}-type patch, consumed 0.185 W to perform $\Delta\zeta = 0.0185$, and the S–M M2814-P1d_{33}-type patch consumed 0.93 W to perform $\Delta\zeta = 0.009$. In comparing the two experimental results, one can conclude that the Advance Cerametrics d_{33} actuator capability outperformed the S–M d_{33}-type patch in terms of the damping and associated power efficiency.

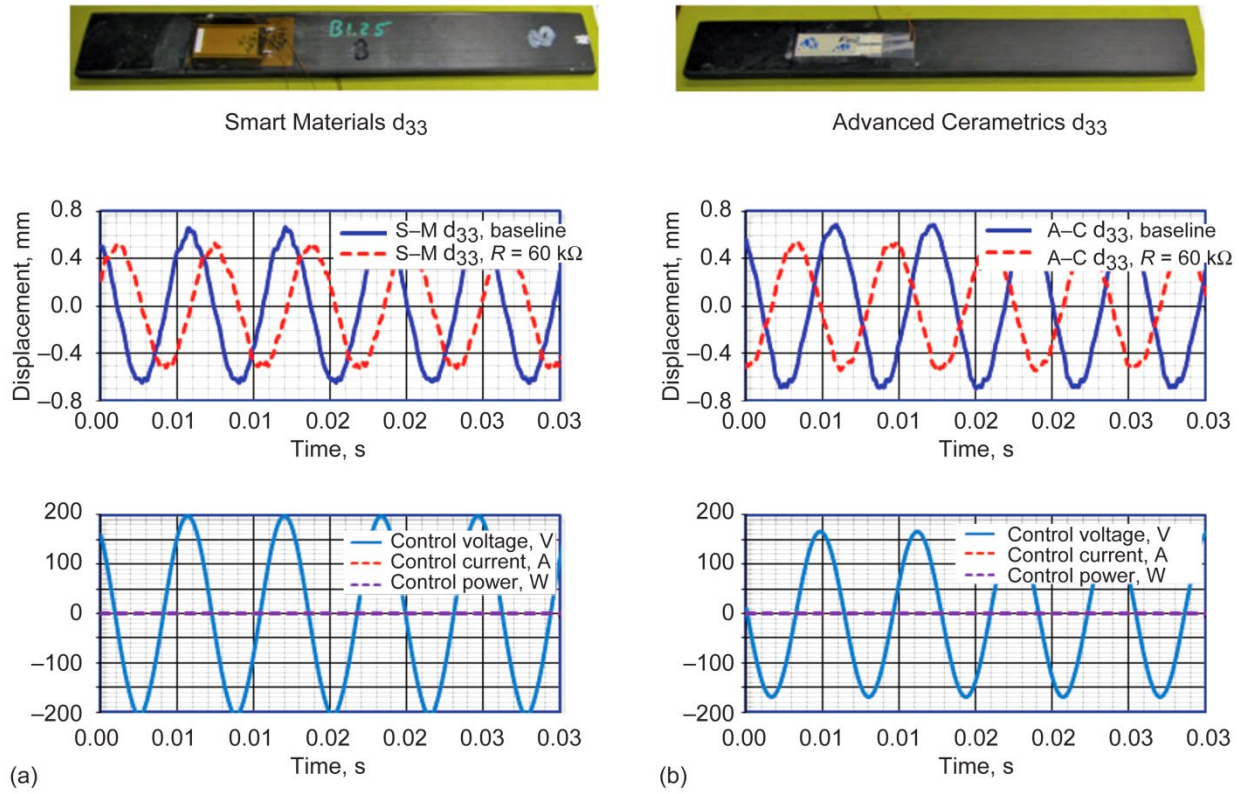

Figure 6.—Control power consumption plots using different piezoelectric patches (narrow beam). (a) Smart Materials (S–M) d_{33}: Tip displacement at 158.3 Hz with 0.99 V to shaker and power required to achieve damping reduction of 0.009. (b) Advanced Cerametrics (A–C) d_{33}: Tip displacement at 157.8 Hz with 0.99 V to shaker and power required to achieve damping reduction of 0.0185.

Similarly, all other type patches were tested on the same narrow and/or other wide beams. All test results are summarized in Table II. The best performing patch was the Advanced Cerametrics d_{33} type. However, the second best candidate, the S–M M2814-P2 d_{31}-type patch, was selected for the subscale GEnx blade damping work because of the availability of the correct size of off-the-shelf patches.

TABLE II.—ACTIVE DAMPING INCREASE RESULTS USING DIFFERENT TYPE PIEZOELECTRIC PATCHES

Beam	Patch type	Piezoelectric actuator	Damping increase, $\Delta\zeta$
Wide	Nonflexible	Midé QP10n d_{31}	0.005
Wide	Nonflexible	Midé QP10w d_{31} (wide)	0.001
Wide	Flexible	Smart Material (S–M) d_{31}	0.012
Wide	Flexible	S–M d_{33}	0.007
Narrow	Flexible	S–M d_{31}	0.012
Narrow	Flexible	S–M d_{33}	0.009
Narrow	Flexible	Advanced Cerametrics d_{33}	0.019

Here, a Midé QPA200 amplifier (±200 V) for all the bench tests. However, since the S–M d_{33} patch can be excited with –500 to +1500 V to generate higher blocking force as shown in Table I, it is expected the d_{33} type would work very well with the higher voltage amplifier. Thus, material selection in this study was constrained by the current QPA200 amplifier.

Nonrotating Testing of Subscale GEnx Blade

The goal of this section is to determine the actuation, sensing, and vibration damping capabilities of the S–M d_{31}-type patches. They were surface mounted to the small-scale GEnx composite fan blade, since the subscale blade thickness was too small to contain the patches. However, the full-size blades will have enough thickness for embedded PE patches. Figure 7 shows the modal stress of the target first bending mode at 0 rpm as determined by ANSYS finite element (FE) code. The star shows the optimum patch locations on the concave and convex sides, respectively.

Now it must be decided on which side of the blade the PE actuator patch must be placed for better damping. A comprehensive FE model of the GEnx blade with surface-mounted PE patches was not developed at the time of this test. Thus, several experimental tests were carried out to identify the optimal actuator and sensor patch configuration. Two identical S–M d_{31}-type patches were placed in an area of high modal stress (Fig. 7) on each side. One patch on the concave side acts as an actuator, and the other on the convex side senses the strain, or vice versa. In the tests, additional accelerometer feedback signal was used to confirm the accuracy and validity of the sensor patch functionality. Notice that an accelerometer is not able to be used in an actual engine. A tiny PE sensor is necessary, which can be easily embedded into the real composite blade.

Test 1 began with a S–M d_{31}-type actuator (PE A) placed on the convex side and another S–M d_{31}-type sensor patch (PE B) placed on the concave side. In this test setup (shown in Fig. 8), a sensing signal of the strain of PE B was fed back to the dSPACE control system, and the control force went to the S–M d_{31} actuator patch (PE A) on the convex side. The transfer function of the strain on the concave side to the base excitation $TF_{\mathrm{PEB\_base}}$ was measured, and $\Delta\zeta = 0.009$ was calculated as shown in Figure 9(a). For comparison purposes, the accelerometer signal was also measured to investigate the blade tip vibration damping when the PE B feedback sensor was used. The transfer function of the accelerometer signal of the tip response on the concave side to the base excitation $TF_{\mathrm{tip\_base}}$ was measured, and $\Delta\zeta = 0.009$ was calculated as shown in Figure 9(b). This test results show that by using a feedback sensor signal of the
PE B, the active damping achievement on PE B is the same as that on the tip displacement.

Figure 7.—Finite element analysis showing optimal patch locations for target first bending mode. (a) Modal stress, concave side. (b) Modal stress, convex side.

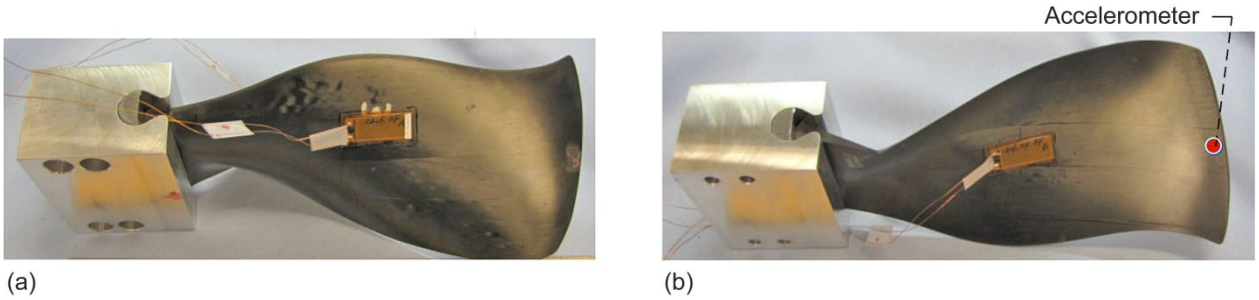

Figure 8.—Smart Material d_{31}-type patch locations on concave and convex sides of blade for Test 1. (a) PE A actuator on convex side. (b) PE B sensor and accelerometer on concave side.

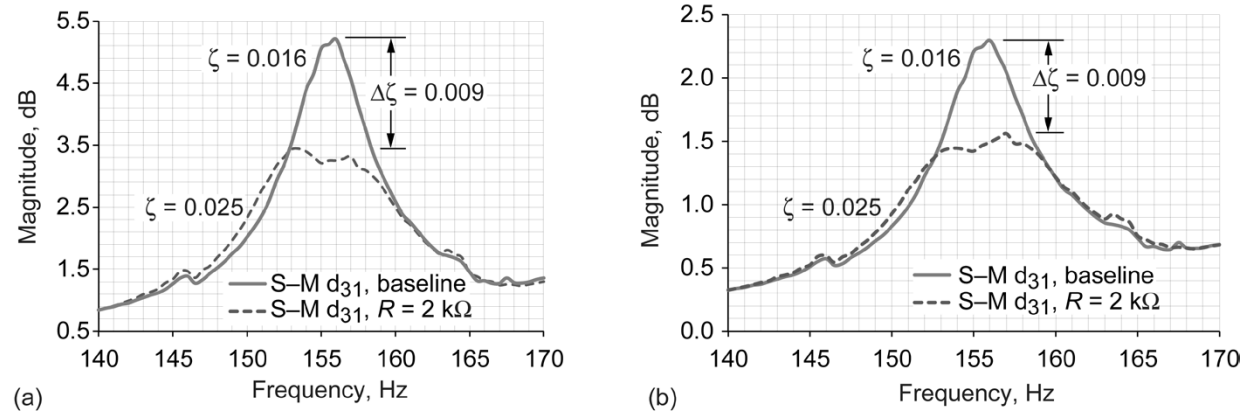

Figure 9.—Bode plots of transfer functions around first bending mode with PE B patch feedback to PE A for Test 1, with the damping ratios ζ and the damping increase Δζ indicated. (a) Transfer function of the sensor piezoelectric to the base, $TF_{\text{PE B\_base}}$. (b) Transfer function of the tip to the base, $TF_{\text{tip\_base}}$.

Similarly, all other configurations were tested and evaluated by the blade tip damping and the PE sensor strain reduction. All experimental testing results are summarized in Table III. Test 4 produced the best damping performance of $\Delta\zeta = 0.021$ from the $TF_{\text{tip\_base}}$, and 0.019 from the $TF_{\text{PEB\_base}}$. Thus, the actuator patch on the concave side of the blade and a small sensing patch on the convex side was the arrangement used for the dynamic spinning test.

TABLE III.—EXPERIMENTAL RESULTS OF INCREASE IN DAMPING RATIO USING DIFFERENT PATCH CONFIGURATIONS

Test	Feedback sensor	Actuator	Transfer function of tip to base, $TF_{\text{tip\_base}}$	Transfer function of sensor piezoelectric (PE) to base, $TF_{\text{PE\_base}}$
1	PE, concave	PE, convex	$\Delta\xi = 0.009$	$\Delta\xi = 0.009$
2	Accelerometer, concave	PE, convex	$\Delta\xi = 0.011$	$\Delta\xi = 0.011$
3	Accelerometer, convex	PE, concave	$\Delta\xi = 0.011$	$\Delta\xi = 0.009$
4	PE, convex	PE, concave	$\Delta\xi = 0.021$	$\Delta\xi = 0.019$

Optimal Topology for Spin Test

Two different patch configurations were tested and evaluated to determine which configuration generated the best performance in terms of vibration damping.

Single-Patch Configuration

Recent FE analysis shows that the strain level on the suction (convex) side of the GEnx blade exceeds the PE patch's durable strain limit for high rotor speed. However, up to 5000 rpm, the FE analysis predicts the safe operation of the patches mounted on the pressure (concave) side, where the strain spreads out at high rotor speed. Thus, the previous optimal configuration as shown in Test 4, where the sensing patch is placed on the suction side, is no longer viable for the spin test. All PE patches must be located in the vicinity of the target placement on the pressure side.

As shown in Figure 10(a), a large actuator (S–M M2814-P2) was glued on the highly strained area, and a small sensing patch (S–M M0714-P2) was lined up along the blade length above the exciter (actuator) patch. In this test setup, $\Delta\zeta = 0.011$ was achieved as shown in Figure 10(b).

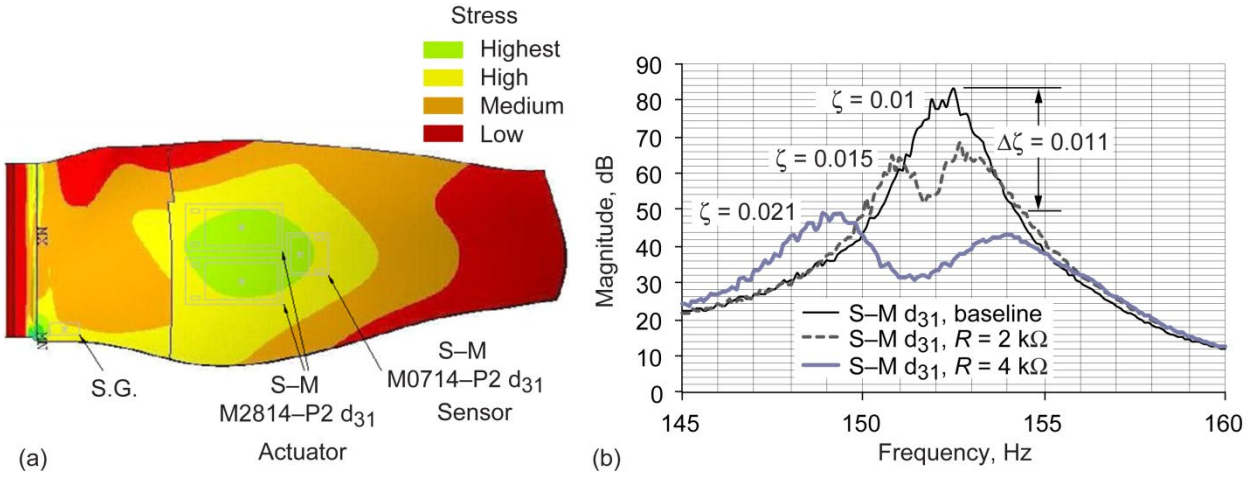

Figure 10.—Optimal single-patch configuration. (a) Smart Material (S–M) d_{31} actuator and sensor locations at highest strain area of blade (S.G. marks the strain gage). (b) Bode plot of transfer functions, $TF_{\text{tip\_base}}$, around first bending mode with damping ratios ζ and increase in damping $\Delta\zeta$ indicated.

Double-Patch Configuration

In this section, a unique double-patch configuration was proposed as one of the optimal topologies. This resulted in substantial improvement over the single-patch configuration. As shown in Figure 11(a), two large actuator patches and one small sensor patch (S–M M0714–P2) are placed around the high modal strain location on the concave (pressure) side. The two large patches can be energized simultaneously to increase the actuating power, or only one actuator can be used at a time, while the other can function as a backup in the event of actuation patch failure.

Two dissimilar S–M d_{31}- (S–M M2814–P2) and d_{33}-type (S–M M2814–P1) materials for Actuator 1 and Actuator 2 (Fig. 11(a)), respectively, were secured on the blade in order to determine which type of patch works better as an actuation patch. Figure 11(b) shows that the S–M d_{31}-type patch achieved $\Delta\zeta = 0.014$, while the S–M d_{33}-type patch achieved $\Delta\zeta = 0.008$. As mentioned earlier, another factor in evaluating the optimal patch selection is the required power consumption for the added damping. As shown in Figure 11(c), the S–M d_{31}-type patch consumed peak-to-peak power of 0.82 V-A to achieve $\Delta\zeta = 0.035$, and the S–M d_{33}-type patch consumed peak-to-peak power of 1.34 V-A to achieve $\Delta\zeta = 0.029$. Evidently, the S–M d_{31}-type patch (S–M M2814–P2) outperformed the d_{33}-type patch (S–M M2814–P1) in terms of damping improvement and associated control power efficiency. This test results reconfirmed the previous experimental results in Table II.

Therefore, we have concluded that the optimal topology of the spin test for the subscale GEnx blade is the double-patch configuration with two S–M d_{31}-type (S–M M2814–P2) actuators and one small S–M d_{31}-type patch (S–M M0714–P2), all bonded on the concave (pressure) side.

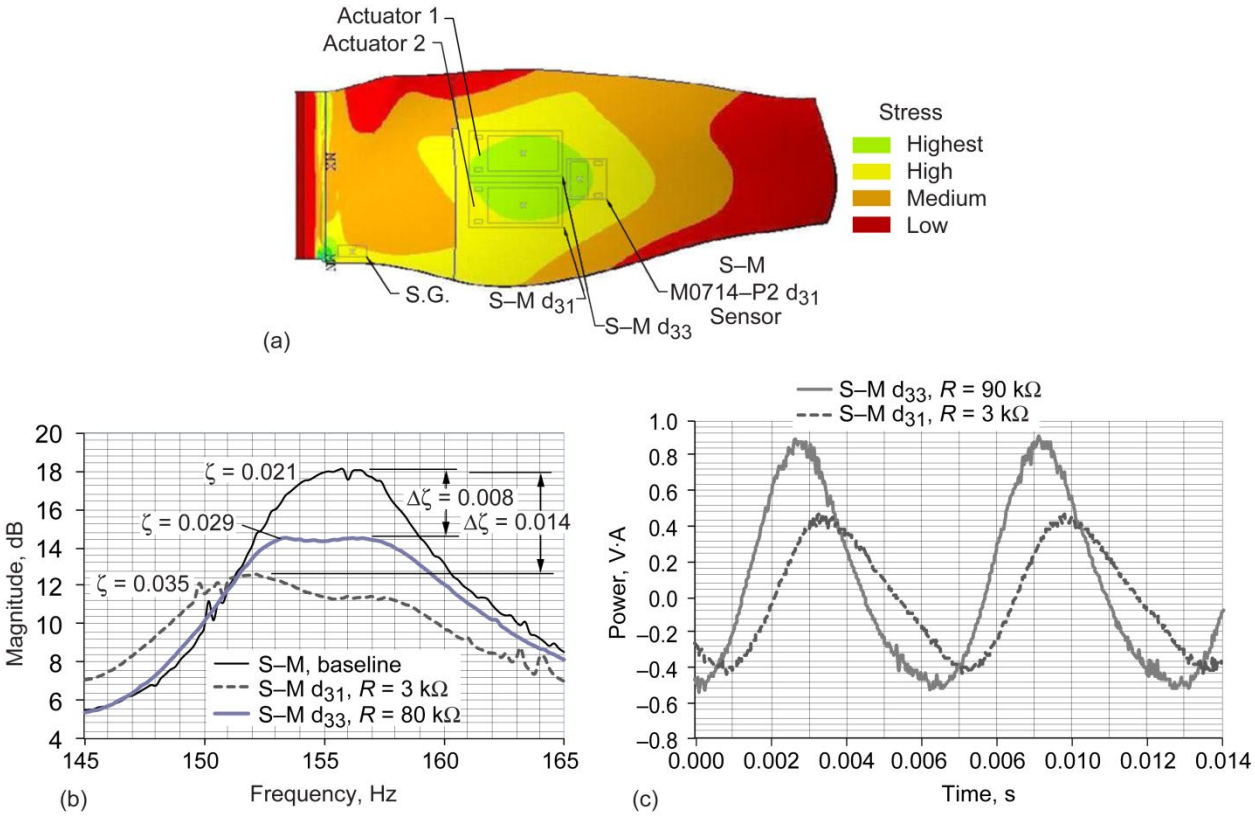

Figure 11.—Optimal double-patch configuration. (a) Locations of two Smart Material (S–M) piezoelectric patch actuators and one sensor. (b) Bode plot of transfer functions TF_{PE31_base} around first bending mode with damping ratios ζ and damping increases $\Delta\zeta$ indicated. (c) Power required to achieve $\Delta\zeta$ using d_{33} and d_{31} actuators.

Spin Test Results

GE Aviation instrumented two test blades with the double-patch configuration described in the previous section, and they were installed in the Dynamic Spin Rig (DSR) (Refs. 16 and 17) facility at NASA Glenn to perform the spin test. The two blades were fixed to a vertical rotor and placed opposite each other (Fig. 12). The rotor was placed in a vacuum tank during operation to reduce the effects of aerodynamic loads. Excitation was provided to the blades through the magnetic bearings that levitated the rotor and blades in five axes. This excitation rotated with the rotor, while maintaining a 90° angle to the blade faces to maximize the excitation force. The magnetic bearings have a bandwidth of 1000 Hz, which is well above the maximum vibration frequency tested. The signals to and from the sensors and actuators traveled through a slip ring, which is located at the bottom of the rotor. The control system and power supplies were all located outside of the spin rig in the control room for safety.

As the shaft rotational speed changes, the blade's natural frequencies will vary due to centrifugal loads so that the tuned controller at 0 rpm is no longer effective. Thus, prior to spinning the blades, a control code modification was needed to address those changing conditions. An adaptive control feature using a lookup table method was added to the closed-loop control system with scheduling variables of inductance and capacitance, which vary as a function of the rotor speed.

It was found that the blades have slightly different resonance frequencies, and coupling exists between the blades through the rotor. This resulted in each blade exhibiting two peaks for each mode as shown in Figure 13(a). The system is inherently a mistuned two-bladed rotor. The test was done using Blade 2 that has the higher response. No accelerometer was installed at the blade base at the time of this test, so the excitation command signal was alternatively used to replace the base acceleration signal for the calculation of the damping ratio.

Finally, the spin test yielded the transfer functions of the PE sensor signal relative to the excitation command signal from 0 to 5000 rpm, in increments of 1000 rpm. Figure 13(b) shows the damping ratio for the baseline open circuit and actively controlled blades using only one actuator (Actuator 2 malfunctioned).

Significant blade damping at 0 rpm was achieved, but the ability to damp decreased as the rotor speed increased. This experimental result agreed with the FE analysis, and is caused by the blade's centrifugal stiffening and by the peak modal strain location changing with the rotor speed. Thus, in practice, the actuator patch location must be decided based on the rotor speed of interest. A more detailed discussion, using additional experimental data is found in Reference 18.

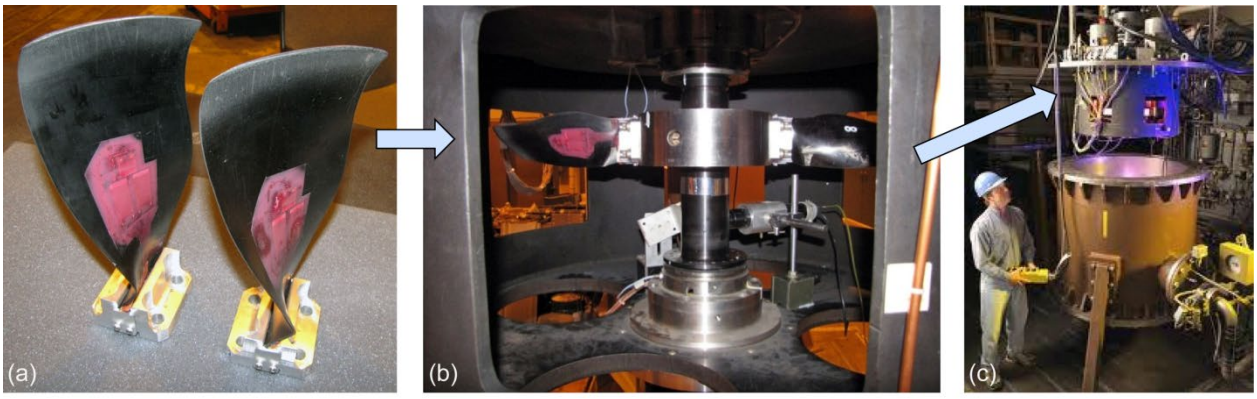

Figure 12.—Blades in the Dynamic Spin Rig. (a) Original blades with piezoelectric patches. (b) Implementation of blades in spin rig rotor. (c) Spin test vacuum chamber.

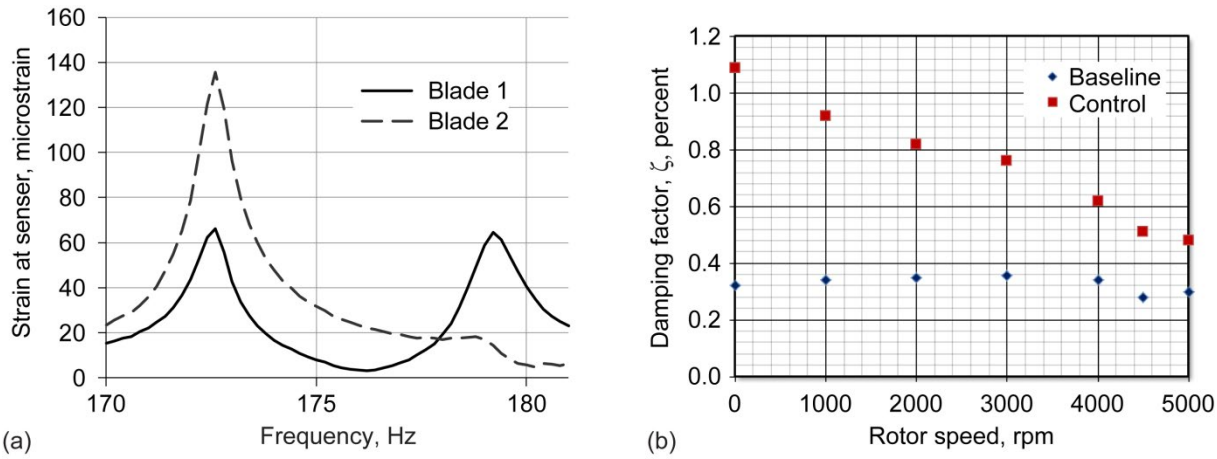

Figure 13.—Spin test results. (a) First bending resonant peaks (Ref. 18) at 0 rpm. (b) Damping ratio for baseline open circuit and actively controlled blades.

Conclusion

An active feedback control technique that emulated the tuned *RLC* circuit was developed. This technique is an alternative to traditional semipassive circuits, which could be problematic in integration of the piezoelectric (PE) damping technology into the rotating fan blades. This active controller enabled our team to demonstrate blade damping in a spin test.

The technique was successfully demonstrated on a variety of GE composite test specimens, resulting in significant resonance damping at the target modes. For the optimal PE patch selection for the test specimens, several commercially available off-the-shelf PE materials were tested through a series of bench-top tests. They were evaluated in terms of damping capability and associated control power requirement, and the Smart Material (S–M) d_{31} type (M2814-P2) was finally selected.

As a result of the experimental comparison study, we finalized the optimal patch topology of the GEnx fan blade with the double-patch configuration, where two identical S–M d_{31}-type actuator patches and one small S–M d_{31}-type sensor patch were placed around the high-modal-strain location on the concave (pressure) side. Finally, successful spin testing up to 5000 rpm was done in Glenn's Dynamic Spin Rig. As anticipated, the damping was reduced as the rotor speed increased because of blade centrifugal stiffening and movement of the area of high modal strain. If damping is required over a particular speed range, the actuator location(s) should be chosen based on high modal strain for that speed range of interest.

However, one question remains unanswered: The actuation patch on the concave (pressure) side of the GEnx achieved more damping than that on the convex (suction) side of the GEnx, which was not expected. This open question must be answered through complete system analysis of an FE model with PE materials.

Future work to improve the PE blade damping must address the following technical challenges:

1. A sophisticated FE model with embedded or surface-mounted PE materials must be developed as a complete analytical tool to simulate and predict the system performance.
2. A higher excitation level must be used to evaluate the PE damping for full-scale fan blades. Possible approaches would be to employ customized patch geometry, a stack of d_{33}-type PE patches, with a high-voltage amplifier and to develop a material with a higher value of electromechanical coupling constant.
3. Implementation of the active control system using mainly operational amplifiers, a digital signal processor (DSP) chip, and a noncontact direct-current (DC) power transmitter from the stationary

frame to the electronic components in the moving frame. An associated system trade study of blade weights reduction versus added electronics weights must be done to justify our efforts to meet the project's ultimate goal.

In addition, there are more challenging technical aspects that must be considered, and more research must be accomplished before implementing the active control system. However, this paper is an attempt at the initial task of proving the feasibility of blade damping.

References

1. Mehmed, Oral; and Kosmatka, John B.: Damping Experiment of Spinning Composite Plates With Embedded Viscoelastic Material. Physics & Process Modeling (PPM) and Other Propulsion R&T, NASA CP–10193, Vol. II, 1997, p. 28.
2. Duffy, Kirsten P.; and Mehmed, Oral: Self-Tuning Impact Dampers for Turbine Blades. Proceedings of the 7th National Turbine Engine High Cycle Fatigue Conference, Palm Beach Gardens, FL, 2002.
3. Duffy, Kirsten P.; Padula II, Santo A.; and Scheiman, Daniel A.: Damping of High-Temperature Shape Memory Alloys. Proc. SPIE, vol. 6929, 2008, p. 69291C.
4. Hagood, N.W.; and von Flotow, A.: Damping of Structural Vibrations With Piezoelectric Materials and Passive Electrical Networks. J. Sound Vib., vol. 146, no. 2, 1991, pp. 243–268.
5. Lesieutre, G.A.: Vibration Damping and Control Using Shunted Piezoelectric Materials. Shock Vib. Dig., vol. 30, no. 3, 1998, pp. 187–195.
6. Cross, Charles J.; and Fleeter, Sanford: Shunted Piezoelectrics for Passive Control of Turbomachine Blading Flow-Induced Vibrations. Smart Mater. Struct., vol. 11, 2002, pp. 239–248.
7. Livet, S., et al.: Numerical and Experimental Optimized Shunted Piezoelectric Circuit. 12th IFToMM World Congress, Besancon, France, 2007.
8. Remington, Paul; Sutliff, Daniel; and Sommerfeldt, Scott: Active Control of Low-Speed Fan Tonal Noise Using Actuators Mounted in Stator Vanes: Part 1 Control System Design and Implementation. AIAA 2003–3190, 2003.
9. Watanabe, Toshinori, et al.: Numerical and Experimental Study of Active Flutter Suppression With Piezoelectric Device for Transonic Cascade. GT2008–51467, 2008.
10. Straub, Friedrich, et al.: SMART Rotor Development and Wind-Tunnel Test. 35th European Rotorcraft Forum, Hamburg, Germany, 2009.
11. Moheimani, S.O. Reza; Halim, Dunant; and Fleming, Andrew J.: Spatial Control of Vibration: Theory and Experiments. Series A, Vol. 10, World Scientific, Singapore, 2003.
12. Moheimani, S.O. Reza; and Fleming, Andrew J.: Piezoelectric Transducers for Vibration Control and Damping. Springer, London, UK, 2006.
13. Choi, Benjamin; Morrison, Carlos; and Duffy, Kirsten: An Active Damping at Blade Resonances Using Piezoelectric Transducers. NASA/TM—2008-215212, 2008.
14. Choi, Benjamin, et al.: Active Vibration Reduction of Titanium Alloy Fan Blades (FAN1) Using Piezoelectric Materials. NASA/TM—2010-216335, 2010.
15. Choi, Benjamin; Morrison, Carlos; and Min, James: A Multi-Mode Blade Damping Control Using Shunted Piezoelectric Transducers With Active Feedback Structure. Presented at the Propulsion, Safety and Affordable Readiness (P–SAR) Conference, Myrtle Beach, SC, 2009.
16. Johnson, Dexter; Brown, Gerald V.; and Mehmed, Oral: A Magnetic Suspension and Excitation System for Spin Vibration Testing of Turbomachinery Blades. NASA/TM—1998-206976, 1998.
17. Choi, Benjamin, et al.: Control Study for Five-Axis Dynamic Spin Rig Using Magnetic Bearings. NASA/TM—2003-212295 (GT2003–38912), 2003.
18. Duffy, Kirsten P., et al.: Active Piezoelectric Vibration Control of Subscale Composite Fan Blades. GT2012–68639, 2012.

REPORT DOCUMENTATION PAGE	Form Approved OMB No. 0704-0188

1. REPORT DATE *(DD-MM-YYYY)*	2. REPORT TYPE	3. DATES COVERED *(From - To)*
01-12-2012	Technical Memorandum	

4. TITLE AND SUBTITLE
Optimal Topology and Experimental Evaluation of Piezoelectric Materials for Actively Shunted General Electric Polymer Matrix Fiber Composite Blades

5a. CONTRACT NUMBER

5b. GRANT NUMBER

5c. PROGRAM ELEMENT NUMBER

6. AUTHOR(S)
Choi, Benjamin, B.; Duffy, Kirsten; Kauffman, Jeffrey, L.; Kray, Nicholas

5d. PROJECT NUMBER

5e. TASK NUMBER

5f. WORK UNIT NUMBER
WBS 561581.02.08.03.43.04.04

7. PERFORMING ORGANIZATION NAME(S) AND ADDRESS(ES)
National Aeronautics and Space Administration
John H. Glenn Research Center at Lewis Field
Cleveland, Ohio 44135-3191

8. PERFORMING ORGANIZATION REPORT NUMBER
E-18220

9. SPONSORING/MONITORING AGENCY NAME(S) AND ADDRESS(ES)
National Aeronautics and Space Administration
Washington, DC 20546-0001

10. SPONSORING/MONITOR'S ACRONYM(S)
NASA

11. SPONSORING/MONITORING REPORT NUMBER
NASA/TM-2012-217631

12. DISTRIBUTION/AVAILABILITY STATEMENT
Unclassified-Unlimited
Subject Categories: 05 and 07
Available electronically at http://www.sti.nasa.gov
This publication is available from the NASA Center for AeroSpace Information, 443-757-5802

13. SUPPLEMENTARY NOTES

14. ABSTRACT
NASA Glenn Research Center, in collaboration with GE Aviation, has begun the development of a smart adaptive structure system with piezoelectric (PE) transducers to improve composite fan blade damping at resonances. Traditional resonant damping approaches may not be realistic for rotating frame applications such as engine blades. The limited space in which the blades reside in the engine makes it impossible to accommodate the circuit size required to implement passive resonant damping. Thus, a novel digital shunt scheme has been developed to replace the conventional electric passive shunt circuits. The digital shunt dissipates strain energy through the load resistor on a power amplifier. General Electric (GE) designed and fabricated a variety of polymer matrix fiber composite (PMFC) test specimens. Investigating the optimal topology of PE sensors and actuators for each test specimen has revealed the best PE transducer location for each target mode. Also a variety of flexible patches, which can conform to the blade surface, have been tested to identify the best performing PE patch. The active damping control achieved significant performance at target modes. This work has been highlighted by successful spin testing up to 5000 rpm of subscale GEnx composite blades in Glenn's Dynamic Spin Rig.

15. SUBJECT TERMS
Piezoelectric transducer; Active damping; Digital shunt; Digital resonant control; Blade damping; Digital passive damping

16. SECURITY CLASSIFICATION OF:			17. LIMITATION OF ABSTRACT	18. NUMBER OF PAGES	19a. NAME OF RESPONSIBLE PERSON
a. REPORT	b. ABSTRACT	c. THIS PAGE			STI Help Desk (email:help@sti.nasa.gov)
U	U	U	UU	24	19b. TELEPHONE NUMBER *(include area code)* 443-757-5802